




Role of mantle indentation in collisional deformation evidenced by deep geophysical imaging of Western Alps

Stéphane Schwartz ¹✉, Yann Rolland^{1,2}, Ahmed Nouibat³, Louise Boschetti^{1,4}, Dorian Bienveignant ¹, Thierry Dumont¹, Marguerite Mathey¹, Christian Sue^{1,5} & Frédéric Mouthereau ⁴

In collision belts, the first-order role of the mantle in localizing deformation has remained elusive, as the resolution of geophysical imaging remains too low to constrain crustal geometry. To address this issue, we geologically interpret a recent high-resolution shear-wave velocity model from ambient-noise tomography of Western Alps. We show that the lower crustal Alpine geometry is highly variable at depth, evolving from a preserved European crustal slab in the South to a smooth crustal root in the North. Moho morphology is controlled by numerous pre-existing major faults reactivated during the Alpine orogeny. Two mantle indenters located above the subducted European plate at different depths appear to control the locus of active deformation. The rigid nature of Adria mantle explains the localization of brittle deformation that is transferred towards the upper crust. The strain-field partitioning results in a combination of strike-slip with either shortening or extension controlled by the anticlockwise rotation of Adria.

¹ISTerre, Université Grenoble Alpes, USMB, CNRS, IRD, UGE, Grenoble, France. ²EDYTEM, Université Savoie Mont Blanc, CNRS, UMR 5204 Le Bourget du Lac, France. ³ITES, Université de Strasbourg, CNRS, UMR 7063 Strasbourg, France. ⁴Géosciences Environnement Toulouse, Université de Toulouse Paul Sabatier, CNRS, IRD, Toulouse, France. ⁵Université de Franche-Comté, Besançon, France. ✉email: stephane.schwartz@univ-grenoble-alpes.fr

Understanding the deep structure of orogenic zones requires high-resolution geophysical data. The correlation between deep seismic imaging, seismicity and surface geology is the best way to decipher the 3D structure of mountain belts. However, this fruitful approach is hampered by the discrepancy in spatial resolution between the various sets of data. The recent shear-wave velocity (V_s) tomography undertaken at the scale of Western Europe^{1,2} allows a reappraisal of the deep structure of the Alpine belt. These geophysical data highlight the role of the crustal geometry in the strain field partitioning observed in the Western Alps^{3,4} (W-Alps). Imaging the lower crustal domains with a high geophysical resolution is critical for the understanding of crust-mantle coupling or decoupling and for localization of seismicity by crustal geological anisotropy^{5,6}.

The crustal-scale geometry of the W-Alps results from the convergence of Europe and Adria plates (Fig. 1a, b) and from the subsequent subduction and collision deformation phases^{7,8}. To the West, the European margin corresponds to the lower plate, which subducted beneath the Adria upper plate to the East. Between these two continental domains, the subduction wedge

was developed by the juxtaposition of High-Pressure (HP) metamorphic rocks including oceanic sediments, crustal fragments originating from the two continental margins and serpentinized mantle corresponding to a mantle wedge^{9,10}. This prism is bounded by two major crustal-scale faults: to the West the Penninic Frontal Thrust (PFT) and to the East the dextral strike-slip Insubric Fault (IF), which represents the southwestern prolongation of the Peri-Adriatic Line¹¹ (Fig. 1b). The European foreland accommodates the convergence through the propagation of a fold-and-thrust belt system in a ‘thin skinned’ tectonic mode associated with the development of Tertiary detrital basins^{12–14}. These basins are further deformed, uplifted and partially eroded during the westward propagation of compressional structures. This compressional deformation is localized at depth along crustal-scale thrusts leading to the exhumation of the External Crystalline Massifs (ECMs) in a ‘thick skinned’ tectonic mode^{15–18}. To the East, above the Adria margin, the Po plain corresponds to a highly subsiding domain bounded by Alpine back-thrusts and Apennine frontal thrusts, which led to the uplift and erosion of parts of its Tertiary basins¹⁹.

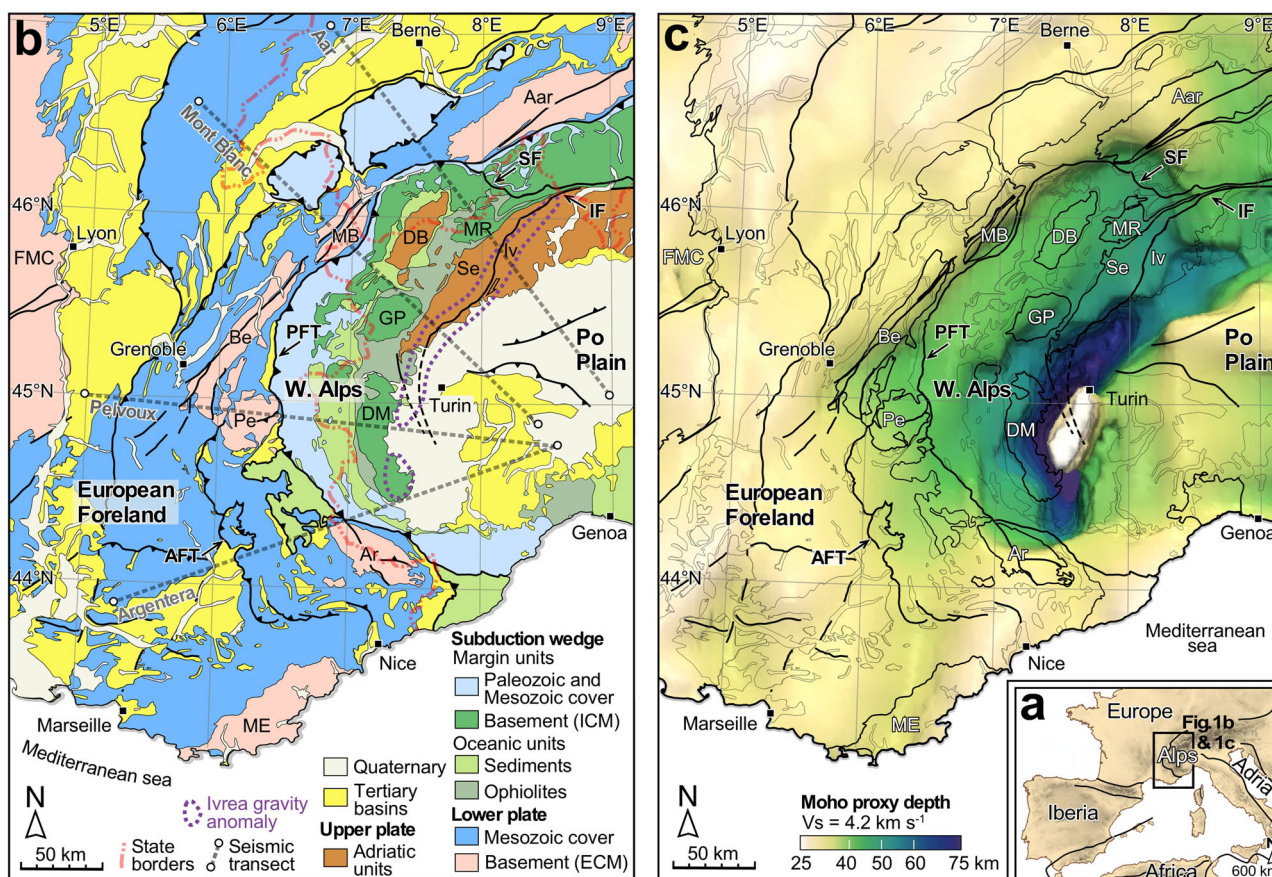


Fig. 1 Geological and tectonic settings of the W-Alps and Moho geophysical map. a sketch map of Western Europe with the main tectonic boundaries and location of the study area. **b** Geological map of the W-Alps with location of the V_s transects shown in Figs. 2 and 4. The Ivrea body gravimetric anomaly is represented by the 0 mGal contour³⁷ (dashed purple line). **c** Moho map computed using a S-wave velocity model from ambient noise tomography¹. The continental crust units of the European plate (lower plate) correspond to a Mesozoic sedimentary cover resting unconformably on a Varsican (350–300 Ma) crystalline basement which outcrops in several External Crystalline Massifs (ECM): Ar Argentera, Be Belledonne, MB Mont-Blanc; Pe Pelvoux, ME Maures-Esterel and in the French Massif Central (FMC). The subduction wedge is located between the two (Europe and Adria) plates and is made of several units from varied paleogeographic origins related to the distal European margin and oceanic units. The distal European margin units are composed of a Paleozoic to Mesozoic sedimentary cover associated with the crystalline basement outcropping in the the internal crystalline massifs (ICM): DM Dora Maira, GP Gran Paradiso, MR Monte Rosa. The oceanic units are represented by sediments (Schistes lustrés) and fragments of oceanic lithosphere (ophiolites). The Adria units (of the upper plate) correspond to a crystalline basement: DB Dent Blanche, Iv Ivrea-Verbano, Se Sesia. Major tectonic structures are also indicated: AFT Alpine Frontal Thrust, IF Insubric Fault, PFT Penninic Frontal Thrust and SF Simplon Fault. The two plates are covered by Tertiary and Quaternary basins.

Despite numerous detailed studies on the Tertiary evolution of the Alps, it still remains difficult to link the crustal-scale structure to the current strain field. The active tectonics displays a complex scheme characterized by an overall strike-slip component with extension in the internal domain of the W-Alps and with compression at the periphery of the belt^{3,4,20}. This scheme is consistent with geodetic measurements, showing significant anticlockwise rotation in the SE part of Adria and slow ($<1 \text{ mm yr}^{-1}$) horizontal motions across the W-Alps belt^{21–23}. It is worth noting that the vertical GPS motions show a significant uplift (up to 2.5 mm yr^{-1}) in the Mont Blanc and Belledonne ECMs of the W-Alps which represent the highest reliefs of the W-Alps. This vertical component progressively vanishes towards the South of the Alpine belt^{22–24}. These motions may result in part from interactions between climate and tectonics (e.g. ^{25–27}), Lithospheric adjustments to deglaciation and erosion likely account for approximately half of the uplift rate. Considering the low convergence rates, the other half should involve a noticeable contribution of mantle-related processes such as the detachment of the European slab and/or asthenospheric upwelling^{26,27}. However, the lack of any precise crustal-scale imagery has prevented any detailed understanding of the localization of the active deformation at depth. Ongoing debate exists on the geometry and continuity of the European slab, as a detached^{28–30} or continuous slab^{31,32}. This debate partly stems from works undertaken on different Alpine cross-sections in Western and Northwestern Alps though, with significantly different lower crustal structures (e.g. ref. ³³).

Here we use a high-resolution crustal-scale Vs model¹, developed in the frame of the AlpArray scientific program³⁴ coupled to the analysis of active deformation represented by the seismicity relocated at crustal scale⁴. This approach enables us to study the location of deformation in relation to crustal scale geometry in order to propose a coherent 3D model of current stress field. The Vs tomography provides an improved image of the Moho geometry beneath the W-Alps, helping to accurately link the crustal geometry to the active deformation pattern. Our results highlight a strong lateral variation of the 3D-crustal structure across the arc, with a preserved crustal slab in the South to a smooth crustal root in the North. The partitioning of deformation in the orogenic prism appears to be controlled by a deep mantle indenter that is split into two units by a major serpentinized sub-vertical structure. The upper mantle unit, located between 20 and 45 km depth, indents the subduction wedge and the Adria margin horizontally and vertically. This process induces the present day extensional seismic activity in the subduction wedge and shortening in the Po plain. The deepest mantle unit, below 45 km, indents horizontally the European slab, propagating compressive deformation into the European foreland.

Results

Moho map. The Moho map (Fig. 1c) corresponds to the 4.2 km s^{-1} isovelocity 3D surface of a recent Vs model obtained with ambient-noise tomography¹ using AlpArray data³⁴. This is the most accurate map of the Moho currently available, with a resolution precise enough to be compared with the main geological units and major tectonic structures that are defined at the surface. This map highlights an eastward deepening of the European Moho in agreement with a subducted European slab beneath the Adria upper plate. The geophysical imagery shows a standard crustal thickness in the forelands ($\sim 30 \text{ km}$). The European Moho (Fig. 1c) exhibits several steps below the ECMs. A more external step (7–8 km) is localized below the Mont Blanc massif along NE–SW trend. This step extends and decreases laterally below the Belledonne massif ($< 5 \text{ km}$). Such features with a

step of 5–12 km are detected along the Alpine arc and underline the accurate shape of the belt. At the both-ends of the W-Alps, South of the Aar and North of the Argentera ECMs respectively, the orientation of the Moho steps shifts to become perpendicular to the belt. In the subduction wedge, S-wave tomography¹ highlights Adria Moho complexity with three superimposed levels. At shallow depth, between 25 and 45 km and in front of the Adria margin, the Moho underlines a 30 km-long mantle promontory isolated within the subduction wedge and corresponds to the Adria Seismic Body (ASB) defined by Nouibat et al.¹. To the East, the ASB is in continuity with a deeper Moho ($>45 \text{ km}$) corresponding to the base of the Adria continental crust. Below the Adria Moho, the European Moho plunges down to $>75 \text{ km}$.

Overall crustal geometry. The crustal geometry is described along four shear-wave tomography transects linked with the surface geology (Fig. 2). The transects are distributed from North to South across the main structures of the arc, and are trending perpendicular to the different ECMs. These transects highlight strong along-strike variations of the crustal geometry. A first order feature to notice is occurrence of Moho steps located at the front of the PFT trace and below the Aar and Mont Blanc ECMs (Fig. 2a, b). The seismic signatures of the European and Adria crusts appear significantly different. The Adria crust shows a homogeneous structure with typical increase of Vs from upper to lower crust, while the European crust shows a strong lateral heterogeneity with domains of low velocity (LVD, $V_s < 3.5 \text{ km s}^{-1}$) in the lower crust.

In addition, in the Northern part of W-Alps (Fig. 2a), the European Moho is smoothed and the crustal European slab is detected to a maximum depth of 60 km, which could be interpreted as a result of former detachment of the European mantle lithosphere^{26,28,30,33} or resulting from a deep Adria mantle indentation producing a crustal stacking at the base of the subduction wedge. In the other transects (Fig. 2b–d) the European slab is continuous down to depths of 80 km. The crustal slab is characterized by a progressive increase in S-wave velocities with depth due to eclogitization and subsequent densification below 45 km depth. Typically for felsic crustal lithologies, eclogite facies shows $V_s > 3.4 \text{ km s}^{-1}$ and up to 4.3 ³². Along the Mont Blanc and Argentera transects (Fig. 2b, d) no significant crustal thickening is observed within the European continental crust (ECC) in the Alpine foreland, West of the PFT. Beneath the subduction wedge, East of the PFT, the crustal geometry shows a more significant crustal thickening to 40–50 km. The shear-wave tomography in the ECC highlights low velocity domains located in the lower crust with velocities $< 3.5 \text{ km s}^{-1}$. The Adria continental crust (ACC) featured by a standard crustal thickness³⁵ (~ 30 – 35 km) below the Po plain, tapers westwards towards the boundary with the subduction wedge, and is outlined by a staircase shape. Within the ACC, shear-wave velocities increase with depth down to the Moho.

The subduction wedge can be divided into two main lithological units (Fig. 2) based on geophysical parameters. The crustal wedge (CW) characterized by $V_s < 3.8 \text{ km s}^{-1}$ is consistent with a tectonic mélange of lithologies from oceanic and continental origins where the continental lithologies are dominant and overprinted by HP–LT metamorphism related to the subduction dynamics (V_s between 3.4 and 3.9)³². The mantle wedge (MW) is characterized by V_s between 3.8 and 4.3 km s^{-1} corresponding to a variably serpentinized mantle³⁶. The Ivrea body gravimetric anomaly^{37,38} fits with the shape of the top of the MW (Fig. 1b, Suppl. Fig. 1).

The shear-wave tomography emphasizes a significant difference between the European and Adria lithospheric mantle units. While the Adria mantle appears homogeneous with high Vs

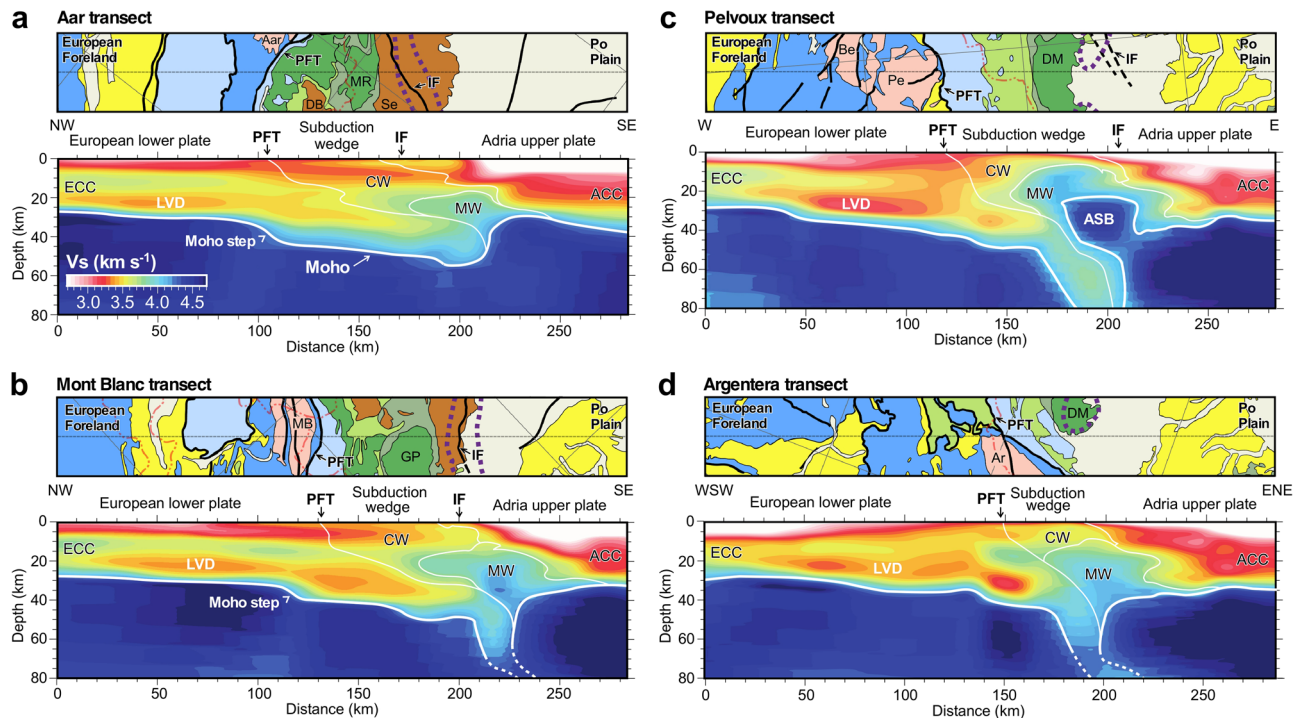


Fig. 2 Vertical shear-wave velocity geophysical transects of W-Alps. First order interpretations of the main structural boundaries delimiting the two plates and the subduction wedge at the crustal scale. The geological map of 20 km on each side of the transects is shown (see Fig. 1b for legend). The Moho is based on isovelocity $V_s = 4.2 \text{ km s}^{-1}$. The location of the main tectonic structures is also indicated (IF Insubric Fault and PFT Penninic Frontal Thrust). The European lower crust shows low velocity domains (LVD) and Moho steps. The boundary between the European Continental Crust (ECC) or the Adria Continental Crust and the subduction wedge is indicated by thin white lines. The subduction wedge is composed of crustal units (CW) overlying a partially serpentinized mantle wedge (MW) highlighted by isovelocities between 3.5 and 4.3 km s^{-1} . The four geophysical transects are located on Fig. 1b, from North to South: (a) Aar; (b) Mont-Blanc; (c) Pelvoux; (d) Argentera.

(> 4.5 km s^{-1}), the European mantle is heterogeneous with V_s variations between 4.2 and 4.5 km s^{-1} . The boundary between the Adria mantle and the subduction wedge (SW) is sharp and steep. As such, it corresponds to the main plate boundary between the European and Adria plates and appears to be offset from the surface trace of the Insubric fault (IF). In the Pelvoux transect (Fig. 2c) the Adria mantle has a complicated and asymmetric shape due to the presence of the ASB. The transition from the ASB to the deep Adria mantle is underlined by a subvertical low velocity zone ($V_s < 4.5 \text{ km s}^{-1}$).

Regional active deformation and strain partitioning. Active deformation, characterized by low magnitude earthquakes ($M_L < 4.5$), appears strongly partitioned at the scale of the Alpine arc (Fig. 3a, b). Seismicity is rather diffuse and shallow (<15 km) within the European foreland, while it appears distributed along two main curved lineaments within the subduction wedge (Fig. 3a). The first one corresponds to the Briançonnais seismic arc located to the East of the PFT and is interpreted as resulting from the relatively shallow (c.a. 10 km depth) extensional reactivation of this main thrust structure³⁹. Further East, the second one clusters at greater depth (down to 25 km), and corresponds to the Piemontais seismic arc showing also mainly extensional earthquakes⁴⁰. The deepest seismicity (>25 km) is still located to the East within the ASB and is rooted in the Adria lithospheric mantle. In a similar way, the strain regime is highly partitioned. The overall deformation, at the scale of the belt, is dominated by a strike-slip regime^{41,42} (Fig. 3b) with domains in transpression on both sides of the belt in the European foreland, Po plain and along the Apennines/Alps junction and a major extensional component within the CW. In this context, the ASB localizes the

main deep compressional activity. Seismic stress inversion computed from focal mechanisms⁴ highlights an overall strike-slip regime with local domains dominated by reverse or normal components (Fig. 3c, Suppl. Fig. 2). The reverse components are located mainly within the deep ASB and more scattered at shallow depth in the frontal part of the ECMs. The normal components are located within the subduction wedge and especially along the Simplon fault and along the Briançonnais and Piemontais seismic arcs. The Briançonnais arc seismicity roots down along the PFT and is related to its extensional reactivation^{39,43}. The Piemontais arc crosscuts the subduction wedge subvertically and is located in the upper part of the mantle wedge.

Discussion

The comparison of the geologically interpreted V_s tomography with the active strain field (Fig. 4) allows to reinterpret the deep structure of the W-Alps and to discuss the role of mantle indentation in collisional deformation related to slab dynamics and / or geological inherited structures.

Mantle indentation and its role on strain localization. Several mantle bodies acting as indenters are identified by the shear-wave tomography. The mantle wedge acts as the uppermost indenter and is related to the Ivrea body gravimetric anomaly^{37,38} and shows seismic signatures of serpentinized mantle³² imbricated with continental and oceanic HP rocks (V_s between 3.8 and 4.3 km s^{-1}). Its upper limit is located at 10 km depth beneath the Dora Maira Internal crystalline massif and Adria units, along the IF structure (Fig. 4b, c).

The main mantle indenter corresponds to the rigid Adria Lithospheric Mantle (ALI), which acts as a plate boundary. ALI

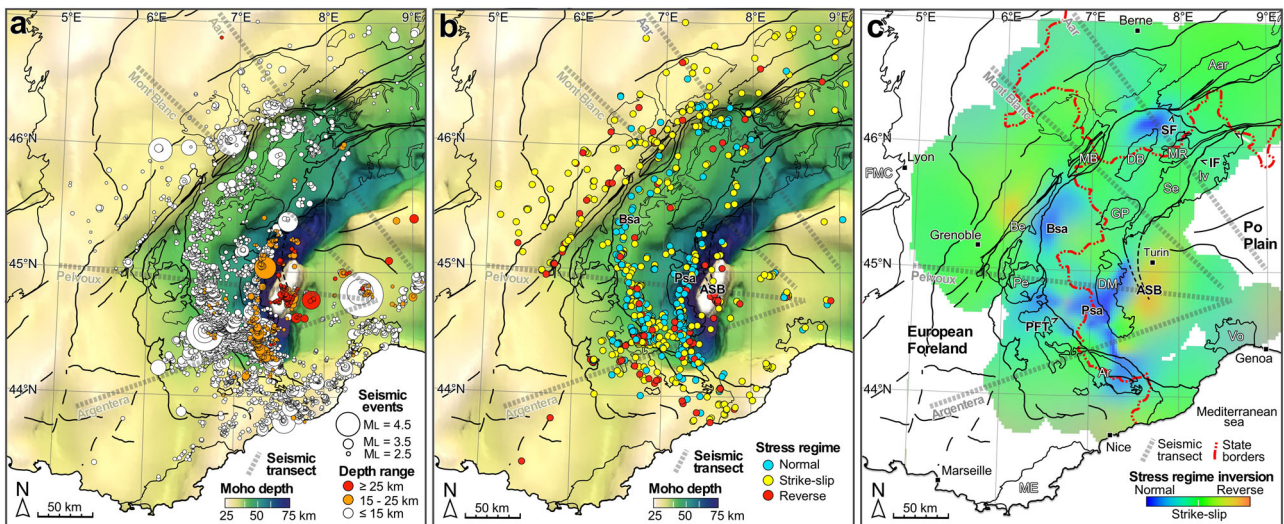


Fig. 3 Seismicity of W-Alps showing magnitudes, depths and stress regimes of earthquakes. **a** Moho map with geological contours with the distribution of epicentres, corresponding magnitudes (M_L) and depth ranges. **b** Moho depth map with stress regimes inferred from earthquake focal mechanisms [4, 60] database. Geophysical transects of Figs. 2 and 4 are shown. **c** Stress field inversion computed from focal mechanisms of earthquakes (modified from [4]). Extensional seismicity clusters along the Simplon fault (SF) in NW Alps and two main seismic lineaments in the SW: the Briançonnais and Piemontais seismic arcs, Bsa and Psa, respectively.

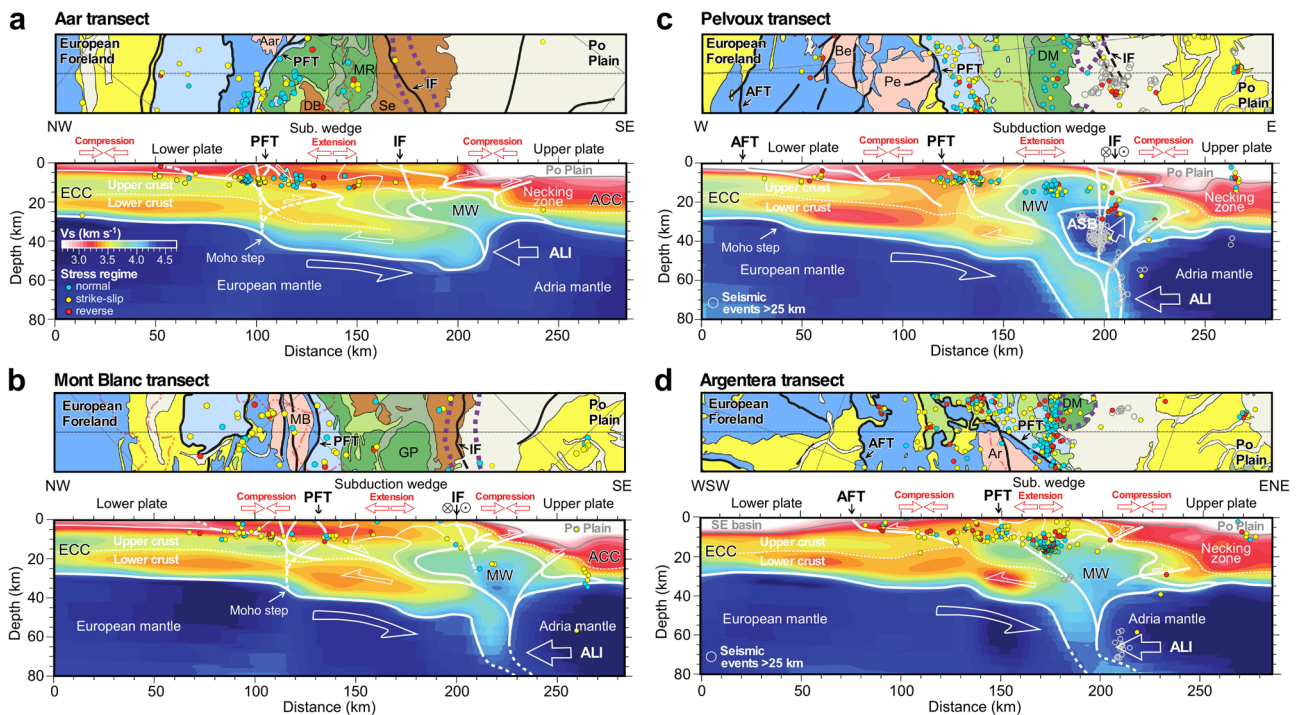


Fig. 4 Shear-wave velocity geophysical transects of W-Alps with seismicity and first order tectonic interpretations. The interpretations of the four transects (from Fig. 2) are indicated by white lines corresponding to main structural boundaries between and within the two plates and the subduction wedge. The main tectonic structures are also represented (IF, Insubric Fault and PFT, Penninic Frontal Thrust). The boundary between upper and lower crust is indicated by a thin dashed line for both the European Continental Crust (ECC) and the Adria Continental Crust (ACC). The thick dashed line above the Moho step corresponds to a vertical crustal-scale fault inherited from the Variscan orogeny. The Adria margin shows a thin continental crust, intensely deformed during the Alpine collision and a preserved crustal domain corresponding to the necking zone of the previously hyperextended margin. The tectonic regimes (compression and extension) are interpreted from focal mechanisms (Suppl. Fig. 2). They are related to the decoupling of the Adria mantle into two superimposed indenters: the deepest indenter corresponds to the Adria Lithospheric Indenter (ALI) and the shallowest corresponds to the Adria Seismic Body (ASB). The main tectonic structures are also indicated (see Fig. 1 for details). The four geophysical transects are located on Fig. 1b, from north to south: **(a)** Aar; **(b)** Mont-Blanc; **(c)** Pelvoux; **(d)** Argentera.

exerts a horizontal compression resulting in slab verticalization and local necking of the European slab where it is continuous (Fig. 4b, d). This process likely triggered crustal slicing and stacking in the Northern part of the W-Alps (Fig. 4a). In the core of the arc (Pelvoux transect, Fig. 4c) ALI was dissected into the ASB, which has been uplifted by the activity of a major steep backthrust. This motion produces a vertical indentation of the subduction wedge and tectonic inversion of the former Adria hyperextended margin⁴⁴. At lithospheric scale, the geometry of ALI and ASB thus corresponds to a positive tectonic flower structure, which is in continuity with the southern segment of the IF. Brittle deformation detected by the seismicity is mainly extensional above and West of the ASB, and is thus interpreted as the expression of a vertical push of this rigid mantle indenter⁴⁵. The uplift of the rigid ASB, and horizontal shortening by the ALI Indenter would explain the vertical exhumation of HP massifs, which mainly occurred in Oligocene to early Miocene in this part of the belt^{45,46}, and stacking of continental eclogites and mantle wedge units below the uplifted Adria margin. Backthrusts to the East of the ASB are no longer active but transpressional tectonics within the ASB indicate a continuation of tectonic activity related to the exhumation of the subduction wedge.

To the West and to the North, in the frontal part of the belt, the compressional component of the overall deformation is interpreted as resulting from a deep compression component transferred to the European slab by the lower indenter (ALI), with a decoupling occurring along the PFT. In front of the ALI indenter, the slab is highly deflected due to this horizontal shortening. This deformation is recorded by the fold-and-thrust belt propagation since >15 Ma¹⁴ in the European foreland. Meanwhile, in response to ALI indentation, the propagation of crustal thickening along a thrust ramp beneath the ECMs produces tectonic inversion of the PFT and subsequent extensional seismic activity along the Briançonnais seismic arc.

Crustal slab geometry at the scale of the W-Alps. The main difference between the northern and SW Alpine cross-sections consists on the presence of a continuous European crustal slab in the South (Fig. 4b–d) and a smooth crustal root in the North (Fig. 4a). In addition, the Northern transects (Fig. 4a, b) exhibit thicker crustal wedge than the southern transects (Fig. 4c, d). In the Aar transect (Fig. 4a) the lower crust is thicker related to the presence of a 100 km large eclogitic root. The general shape of the eclogitic root, with a flat geometry and the absence of any residual slab suggests an isostatic reequilibration of the collisional belt in response to the stacking of crustal material scrapped from the European slab by ALI mantle indenter. The difference between the North and the South transects can be explained by the initial shape of the European margin. In the Northern Alps, the crustal slab thickness was reduced due to the presence of an oceanic basin (the Valais Ocean)⁴⁷ which did not exist in the Central and Southern part of the arc⁴⁸. In contrast, in the SW Alps, the presence of a continuous continental margin⁴⁹ and of the ASB indenter at shallow depth. Therefore, the continental crust slab has remained continuous only in the SW and shows significant pinching deformation at a depth >60 km due to horizontal shortening in front of ALI.

Geological inheritance and reactivation. The role of geological inheritance in the belt structure is well shown by the geometry of the Adria margin (Fig. 4a–d). The previously thinned to hyperextended margin of Adria is highlighted by the presence of a thin continental crust (10 to 15 km) passing laterally to a standard crustal thickness across a necking zone structure corresponding to the boundary of the hyperextended margin⁵⁰. The former

normal faults of the Adria margin were inverted and uplifted by the rise of the ASB. This reactivation resulted in a positive flower-type structure. Stacking of internal prism units below the Adria margin implies a crust - mantle decoupling.

Considering the European crust, the occurrence of low V_s velocity domains in the lower crust is not related with Alpine tectonics because their extent largely exceeds the limits of the belt. Their origin may be instead related with the late stages of the Variscan orogeny and with the emplacement of more felsic migmatite crust during the development of metamorphic core complexes similar to the Montagne Noire dome⁵¹.

Finally, the W-Alps belt appears to be thickened only in its Internal part (subduction wedge), and shows a normal crustal thickness (~30–35 km) in its External part (European foreland). This transition is accommodated by a sharp Moho step likely corresponding to a fault zone localized below the Belledonne and Mont Blanc ECMs (Fig. 4a, b). This Moho step is interpreted as the reactivation of the inherited ‘East Variscan Shear Zone’ or EVSZ^{52–54}. A similar step also occurs to the South beneath the EVSZ of Argentera ECM^{55,56}. Further, along the Pelvoux and Argentera transects (Fig. 4c, d) moderate crustal thickening (35–40 km) occurs in the external part related to the development of the Alpine Frontal Thrust or AFT¹⁷, which, to the East, roots onto the top of the lower crust. The motion on the AFT is controlled by the ALI and ASB indentation.

3D seismotectonic model of W-Alps. The partitioning of W-Alps deformation is evidenced between purely compressional deformation in the AFT, transpressional strike-slip deformation along the EVSZ and IF, and transtensional to extensional deformation along the Piemontais and Briançonnais seismic arcs. In an overall strike-slip deformation context, this partitioning results from a mantle indentation process that accommodates displacements imposed by the current NW / SE convergence associated with a low anticlockwise rotation of Adria^{4,20–23} (Fig. 5a). Mantle indentation induced by the more rigid Adria lithosphere is shared into two units (ALI and ASB) by a major serpentinized steep W-dipping tectonic structure (Fig. 5b). The upper unit (ASB), located between 20 and 45 km below the surface, indents vertically the subduction wedge and results in the exhumation of the HP rocks. This vertical indentation is also responsible for the extension along the Piemontais seismic arc and the backthrusting of the previously thinned Adria margin. The deepest unit (ALI) indents horizontally the European slab, propagating compressive deformation into the European foreland by the activation of the AFT. At the back of the crustal-scale AFT structure, the PFT is reactivated in extension with the development of the Briançonnais seismic arc. Given the arcuate shape of W-Alps, the Briançonnais arc merges into the dextral transpressional NE / SW inherited vertical EVSZ. A similar transition from dextral to extensional deformation occurs along the Simplon Fault (SF) to the North. The motor of the Adria anticlockwise rotation corresponds to the far field Mediterranean tectonics dominated by the subduction of the Adria plate⁵⁷.

Methods

Crustal-scale shear-wave velocity imaging. The 3D Moho map and velocity cross-sections in Figs. 1–5 are computed from a recent 3D high-resolution shear-wave model (V_s model) from ambient-noise tomography (ANT)¹ that used data from the AlpArray network³⁴, dense temporary experiments in W-Alps (Cifalps 1-2^{58,59}) and all permanent seismic networks available throughout Western Europe during 2015–2019. This velocity model was validated by receiver functions (RFs) and controlled-source seismic (CSS) available for the W-Alps^{1,59}, which makes it

the most well-constrained and the highest resolution (15 km laterally and 1–5 km at depth) Vs model to date. Based on the preliminary comparison of this ANT model with receiver functions along the Cifalps 1 profile¹, a coherent geological model was proposed. This geological framework served as a basis for geological reconstruction of the whole W-Alps along four geological transects presented in this paper. We use the 4.2 km s⁻¹ isovelocity as a proxy for the Moho since [1, 59] have shown that both the latter and the 4.3 km s⁻¹ isovelocity are well-suited to delineate the Moho beneath the European and Adriatic forelands. These isovelocity values are also suitable for tracking the deepening of the Moho associated with subduction of the European lithosphere, in agreement with the RFs and CSS data. In this paper we choose the 4.2 km s⁻¹ because it is more stable at large depths, particularly beneath the subduction wedge.

Seismotectonics. Additionally, we use the available seismotectonic data encompassing the Western Alps (Fig. 3). We combine earthquake hypocenters and focal mechanisms from two existing databases^{4,60}. The first database⁴ includes more than 2200 focal mechanisms computed for earthquakes recorded between 1989 and 2013, and the second one⁶⁰ includes more than 100 focal mechanisms computed for earthquakes recorded between 1986–2016. We only kept events with a magnitude higher than 2, which corresponds to more than 6900 hypocenters in total (Fig. 3a), of which more than 990 have focal mechanism solutions (Suppl. Fig. 2). In Fig. 4, we project the hypocenters and focal mechanisms at depth onto the four transects of Fig. 2, with distances of 20 km on either side perpendicular of the transect tracks shown in Fig. 3. Finally, we use a continuous 2D map showing the spatial variations in deformation modes derived by [4] (Fig. 3c). This map was obtained by interpolating the mode of deformation around the bend of the W-Alps. The mode of deformation is characterized by 3 endmembers corresponding to extensional, compressional or strike-slip respectively. The intermediate states could be represented in ternary diagrams⁶¹ and are controlled by the plunge angles of both the pressure (P) and tension (T) axes of the focal mechanisms. The mode of deformation, represented on map (Fig. 3c) is obtained by a cross-interpolation of the two plunge angles based on a Bayesian method⁴. This method provides an interpolation of multi-dimensional fields (3 dimensions in our case) for heterogeneous density of data, as the focal mechanisms are not homogeneously distributed throughout the Alps. This approach represents a significant improvement with respect to previous attempts to synthesize Alpine seismotectonics⁴⁰.

Data availability

Together with this paper, we provide the data repository available at <https://doi.org/10.18709/perscido.2023.12.ds403> that contains: (1) the 3D Moho map and Vs transects from Nouibat et al. (2022), (2) earthquake hypocenters and focal mechanisms from the database of Mathey et al. (2021), and (3) the Bayesian solution of the distributions of P, T and B axis plunges from Mathey et al. (2021), that can be used to reconstruct the stress regime map. This paper uses also earthquake hypocenters and focal mechanisms from the dataset of Eva et al. (2020), which are available at <https://doi.org/10.17632/5jp698sf2p.1>.

Received: 29 July 2023; Accepted: 12 December 2023;
Published online: 05 January 2024

References

- Nouibat, A. et al. Lithospheric transdimensional ambient-noise tomography of W-Europe: implications for crustal-scale geometry of the W-Alps. *Geophys. J. Intern.* **229**, 862–879 (2022).
- Nouibat, A. et al. Ambient-noise tomography of the Ligurian-Provence basin using the AlpArray onshore-offshore network: Insights for the oceanic domain structure. *J. Geophys. Res. Solid Earth* **127**, 86634 (2022).
- Delacou, B. et al. Present-day geodynamics in the bend of the western and central Alps as constrained by earthquake analysis. *Geophys. J. Int.* **158**, 753–774 (2004).
- Mathey, M. et al. Present-day geodynamics of the Western Alps: new insights from earthquake mechanisms. *Solid Earth* **12**, 1661–1681 (2021).
- Lardeaux, J. M. et al. A crustal-scale cross-section of the south-western Alps combining geophysical and geological imagery. *Terra Nova* **18**, 412–422 (2006).
- Malusà, M. et al. Earthquakes in the western alpine mantle wedge. *Gondwana Res.* **44**, 89–95 (2017).
- Polino, R. et al. Tectonic erosion at the Adria margin and accretionary processes for the cretaceous orogeny of the Alps. *Mem. Soc. Geol. Fr.* **156**, 345–367 (1990).
- Dumont, T. et al. Structural and sedimentary records of the Oligocene revolution in the Western Alpine arc. *J. Geodyn.* **56–57**, 18–38 (2012).
- Schwartz, S. et al. Late tectonic and metamorphic evolution of the Piedmont accretionary wedge (Queyras Schistes lustrés, western Alps): evidences for tilting during Alpine collision. *Geol. Soc. Amer. Bull.* **121**, 502–518 (2009).
- Agard, P. Subduction of oceanic lithosphere in the Alps: selective and archetypal from (slow-spreading) oceans. *Earth Sci. Rev.* **214**, 103517 (2021).
- Schmid, S. M. et al. Ivrea mantle wedge, arc of the Western Alps, and kinematic evolution of the Alps–Apennines orogenic system. *Swiss J. Geosci.* **110**, 581–612 (2017).
- Ford, M. et al. Tertiary foreland sedimentation in the Southern Subalpine chains, SE France: a geodynamic appraisal. *Basin Res.* **11**, 315–336 (1999).
- Kalifi, A. et al. Chronology of thrust propagation from an updated tectono-sedimentary framework of the Miocene molasse (western Alps). *Solid Earth* **12**, 2735–2771 (2021).
- Bilau, A. et al. The tertiary structuration of the Western Subalpine foreland deciphered by calcite-filled faults and veins. *Earth Sci. Rev.* **236**, 104270 (2022).
- Jourdon, A. et al. Style of Alpine tectonic deformation in the Castellane fold-and-thrust belt (SW Alps, France): insights from balanced cross-sections. *Tectonophysics* **633**, 143–155 (2014).
- Bellahsen, N. et al. Collision kinematics in the western external Alps. *Tectonics* **33**, 1055–1088 (2014).
- Schwartz, S. et al. Foreland exhumation controlled by crustal thickening in the Western Alps. *Geology* **45**, 139–142 (2017).
- Girault et al. Exhumation of the Western Alpine collisional wedge: new thermochronological data. *Tectonophysics* **822**, 229155 (2022).
- Mosca, P. et al. New data for the kinematic interpretation of the Alps–Apennines junction (Northwestern Italy). *Int. J. Earth Sci.* **99**, 833–849 (2010).
- Rolland, Y. et al. Bridging the gap between long-term orogenic evolution (>10 Ma Scale) and geomorphological processes that shape the Western Alps: insights from combined dating approaches. *Geosciences* **12**, 393 (2022).
- Walpersdorf, A. et al. Does long-term GPS in the Western Alps finally confirm earthquake mechanisms? *Tectonics* **37**, 3721–3737 (2018).
- Serpelloni, E. et al. Vertical GPS ground motion rates in the Euro-Mediterranean region: new evidence of velocity gradients at different spatial scales along the Nubia-Eurasia plate boundary. *J. Geophys. Res. Solid Earth* **118**, 6003–6024 (2013).
- Nocquet, J. et al. Present-day uplift of the western Alps. *Sci. Rep.* **6**, 28404 (2016).
- Mathey, M. et al. Spatial heterogeneity of uplift pattern in the western European Alps revealed by InSAR time-series analysis. *Geophys. Res. Lett.* **49**, e2021GL095744 (2022).
- Champagnac, J. D. et al. Quaternary erosion-induced isostatic rebound in the western Alps. *Geology* **35**, 195–198 (2007).
- Fox, M. et al. (2015). Rapid exhumation in the Western Alps driven by slab detachment and glacial erosion. *Geology* **43**, 379–382 (2015).
- Sternai, P. et al. Present-day uplift of the European Alps: evaluating mechanisms and models of their relative contributions. *Earth Sci. Rev.* **190**, 589–604 (2019).
- Lippitsch, R. et al. Upper mantle structure beneath the Alpine orogen from high-resolution teleseismic tomography. *J. Geophys. Res. Solid Earth* **108**, 89961 (2003).
- Handy, M. R. et al. Orogenic lithosphere and slabs in the greater Alpine area—interpretations based on teleseismic P-wave tomography. *Solid Earth* **12**, 2633–2669 (2021).
- Paffrath, M. et al. Imaging structure and geometry of slabs in the greater Alpine area – a P-wave travel-time tomography using AlpArray seismic network data. *Solid Earth* **12**, 2671–2702 (2021).
- Zhao, L. et al. Continuity of the Alpine slab unraveled by high-resolution P wave tomography. *J. Geophys. Res. Solid Earth* **121**, 8720–8737 (2016).
- Malusà, M. et al. The deep structure of the Alps based on the CIFALPS seismic experiment: a synthesis. *Geochem. Geophys. Geosyst.* **55**, e2020GC009466 (2021).

33. Schmid, S. M. & Kissling, E. The arc of the western Alps in the light of geophysical data on deep crustal structure. *Tectonics* **19**, 62–85 (2000).
34. Hetényi, G. et al. The AlpArray seismic network: a large-scale European experiment to image the Alpine Orogen. *Surv. Geophys.* **39**, 1009–1033 (2018).
35. Wedepohl, K. H. The composition of the continental crust. *Geochim. Cosmochim. Acta.* **59**, 1217–1232 (1995).
36. Grevemeyer, I. et al. Episodic magmatism and serpentinized mantle exhumation at an ultraslow-spreading centre. *Nature Geosci.* **11**, 444–448 (2018).
37. Berkheimer, H. Topographie des Ivrea-KGrpers, abgeleitet aus seismischen und gravimetrischen Daten. *Schweiz. Mineral. Petrograph. Mitt.* **48**, 235–246 (1968).
38. Bigi, G., Cosentino, D., Parotto, M., Sartori, R. & Scandone, P. Structural model of Italy and gravity map. *Quad. Ric. Sci.* **114**, 211–235 (1990).
39. Tricart, P. & Sue, C. Faulted backfold versus reactivated backthrust: the role of inherited structures during late extension in the frontal Piémont nappes east of Pelvoux (Western Alps). *Intern. J. Earth Sci.* **95**, 827–840 (2006).
40. Sue, C. et al. Mechanical behavior of western alpine structures inferred from statistical analysis of seismicity. *Geophys. Res. Lett.* **29**, 65–1 (2002).
41. Truttmann, S., Diehl, T. & Herwegh, M. Hypocenter-based 3D Imaging of active faults: method and applications in the Southwestern Swiss Alps. *J. Geophys. Res. Solid Earth* **128**, e2023B026352 (2023).
42. Bauve, V. et al. Long-lasting transcurrent tectonics in SW Alps evidenced by Neogene to present-day stress fields. *Tectonophysics* **621**, 85–100 (2014).
43. Bilau, A. et al. Extensional reactivation of the Penninic frontal thrust 3 Myr ago as evidenced by U–Pb dating on calcite in fault zone cataclasis. *Solid Earth* **12**, 237–251 (2021).
44. Manatschal, G. et al. Tectono-magmatic evolution during the extensional phase of a Wilson Cycle: a review of the Alpine Tethys case and implications for Atlantic-type margins. *Italian J. Geosci.* **142**, 5–27 (2023).
45. Rolland, Y. et al. Syn-convergence extension, vertical pinching and contrasted metamorphic units on the western edge of the Gran Paradis massif (French-Italian Alps). *Geodinam. Acta.* **13**, 133–148 (2000).
46. Tricart, P. et al. Evidence of synextension tilting and doming during final exhumation from analysis of multistage faults (Queyras Schistes lustrés, Western Alps). *J. Struct. Geol.* **26**, 1633–1645 (2004).
47. Rosenbaum, G. & Lister, G. S. The Western Alps from the Jurassic to Oligocene: spatio-temporal constraints and evolutionary reconstructions. *Earth Sci. Rev.* **69**, 281–306 (2005).
48. Dumont, T. et al. Cross-propagation of the western Alpine orogen from early to late deformation stages: evidence from the Internal Zones and implications for restoration. *Earth Sci. Rev.* **232**, 1–32 (2022).
49. Célini, N. et al. Rift thermal inheritance in the SW Alps (France): insights from RSCM thermometry and 1D thermal numerical modelling. *Solid Earth* **14**, 1–16 (2023).
50. Mohn, G. et al. Necking of continental crust in magma-poor rifted margins: evidence from fossil Alpine Tethys margins. *Tectonics* **31**, TC1012 (2012).
51. Vanderhaeghe, O. Migmatites, granites and orogeny: Flow modes of partially-molten rocks and magmas associated with melt/solid segregation in orogenic belts. *Tectonophysics* **477**, 119–134 (2009).
52. Corsini, M. & Rolland, Y. Late evolution of the southern European Variscan belt: exhumation of the lower crust in a context of oblique convergence. *C. R. Geosci.* **341**, 214–223 (2009).
53. Simonetti, M. et al. Transpressive deformation in the southern European Variscan belt: new insights from the Aiguilles rouges massif (Western Alps). *Tectonics* **39**, e2020TC006153 (2020).
54. Vanardois, J. et al. Deformation, crustal melting and magmatism in the crustal-scale East-Variscan shear zone (Aiguilles-Rouges and Mont-Blanc massifs, Western Alps). *J. Struct. Geol.* **163**, 104724 (2022).
55. Simonetti, M., Carosi, R., Montomoli, C., Law, R. D. & Cottle, J. M. Unravelling the development of regional-scale shear zones by a multidisciplinary approach: the case study of the Ferrière-Mollières Shear Zone (Argentera Massif, Western Alps). *J. Struct. Geol.* **149**, 104399 (2021).
56. Sanchez, G. et al. Dating low-temperature deformation by $^{40}\text{Ar}/^{39}\text{Ar}$ on white mica, insights from the Argentera-Mercantour Massif (SW Alps). *Lithos* **125**, 521–536 (2011).
57. Jolivet, L. & Facenna, C. Mediterranean extension and Africa-Eurasia collision. *Tectonics* **19**, 1095–1106 (2000).
58. Zhao, L. et al. First seismic evidence for continental subduction beneath the Western Alps. *Geology* **43**, 815–818 (2015).
59. Paul, A. et al. Along-strike variations in the fossil subduction zone of the Western Alps revealed by the CIFALPS seismic experiments and their implications for exhumation of (ultra-) high-pressure rocks. *Earth Planet. Sci. Lett.* **598**, 117843 (2022).
60. Eva, E. et al. Seismotectonics at the transition between opposite-dipping slabs (Western Alpine Region). *Tectonics* **39**, e2020TC006086 (2020).
61. Frohlich, C. Triangle diagrams: ternary graphs to display similarity and diversity of earthquake focal mechanisms. *Phys. Earth Planet. Inter.* **75**, 193–198 (1992).

Acknowledgements

We thank the Editor, as well as Emanuel Kästle and two anonymous reviewers, for their thoughtful feedback, which has substantially improved the manuscript. This work is based on PhD works of A.N. co-funded by the RGF program (Référentiel Géologique de la France (<http://rgf.brgm.fr>)) and by SEISCOPE consortium (<http://seiscope2.osug.fr>). The authors thank discussions with M. Malusà, N. Bellahsen, D. Marquer, L. Jolivet, C. Rosenberg and L. Labrousse in the frame of the RGF project.

Author contributions

Conceptualization: S.S., Y.R. and A.N. Methodology and data acquisition: A.N., C.S. and M.M. Investigation: S.S., Y.R. and A.N. Visualization: S.S., Y.R. and A.N. Writing—original draft: S.S., Y.R., A.N., L.B., D.B., T.D. and F.M. Writing—review and editing: S.S., Y.R., A.N., L.B., D.B., T.D., F.M., C.S. and M.M.

Competing interests

The authors declare no competing interests.

Additional information

Supplementary information The online version contains supplementary material available at <https://doi.org/10.1038/s43247-023-01180-y>.

Correspondence and requests for materials should be addressed to Stéphane Schwartz.

Peer review information *Communications Earth & Environment* thanks Emanuel Kästle and the other, anonymous, reviewer(s) for their contribution to the peer review of this work. Primary Handling Editors: Kim Welford, Joe Aslin and Aliénor Lavergne. A peer review file is available.

Reprints and permission information is available at <http://www.nature.com/reprints>

Publisher's note Springer Nature remains neutral with regard to jurisdictional claims in published maps and institutional affiliations.



Open Access This article is licensed under a Creative Commons Attribution 4.0 International License, which permits use, sharing, adaptation, distribution and reproduction in any medium or format, as long as you give appropriate credit to the original author(s) and the source, provide a link to the Creative Commons licence, and indicate if changes were made. The images or other third party material in this article are included in the article's Creative Commons licence, unless indicated otherwise in a credit line to the material. If material is not included in the article's Creative Commons licence and your intended use is not permitted by statutory regulation or exceeds the permitted use, you will need to obtain permission directly from the copyright holder. To view a copy of this licence, visit <http://creativecommons.org/licenses/by/4.0/>.

© The Author(s) 2024